Adjustable Dual Beam Wireless Base Station Antenna

Senglee Foo, Member, *IEEE*, Bill Vassilakis, Senior Member, *IEEE*

Powerwave Technologies, 1801 E. St. Andrew Place, Santa Ana, CA, 92705
Email: Senglee.Foo@pwav.com, Tel: 714-388-7338

***Abstract* — This article presents a multi-column array and a beam forming circuit that produces two overlapping beams with high efficiency and adjustable beam patterns for wireless base station applications. The proposed antenna is an adjustable cylindrical sector array comprising of three separate columns of linear array. This structure allows forming of two overlapping beams with amplitude and phase excitations which can be implemented using a compact and low loss circuit. The adjustable offset displacement for the center column array allows refinement and adjustment of pattern characteristics of the two overlapping beams. This method results in beam split loss of less than 0.5dB in comparison to a single beam case. Performance parameters such as the beam cross-over loss and pattern discrimination between beams can also be adjusted in-situ for optimum operation.**

***Index Terms* — Beam forming network, dual beam, multi-beam array, base station antenna, smart antenna.**

I. Introduction

In a high-capacity wireless network, cell coverage in a sector may require narrower beam patterns to meet the demand capacity. In such scenarios, the sector may be better served using two overlapping beams of narrower beamwidth. A multi-column array is typically used to form the multiple beams using a combination of hybrids, couplers and phase shifters [1] [2]. This general beam forming method often incurs an additional front-end loss as a result of circuit path losses and signal split between beams. Furthermore, a general beam forming method often requires multiple crossing between input feed lines, which can cause difficulties in the actual beam-forming circuit implementation.

This paper presents a compact, low-cost beam forming structure for use in efficient beam forming of two overlapping beams within a cellular sector. This method allows increase in an overall network capacity by using multiple columns of linear array arranged on a cylindrical curvature. This arrangement results is an amplitude and phase excitations taper which can be implemented using a simple and low-loss beam forming network. This method produces two symmetrical beams with respect to the azimuth boresight. Radiation patterns of the two beams are overlapped in the manner that the coverage of the cellular sector can be optimized using the adjustable beam array.

II. 3-column dual beam Array

The proposed antenna is a cylindrical sector array, which can be perceived as a superposition of two partially-filled ring arrays. The azimuth pattern of the two-ring circular array can be varied by adjusting the relative dimension of the radiuses of the rings. Fig. 1 depicts the theoretical model of a general two-ring array.

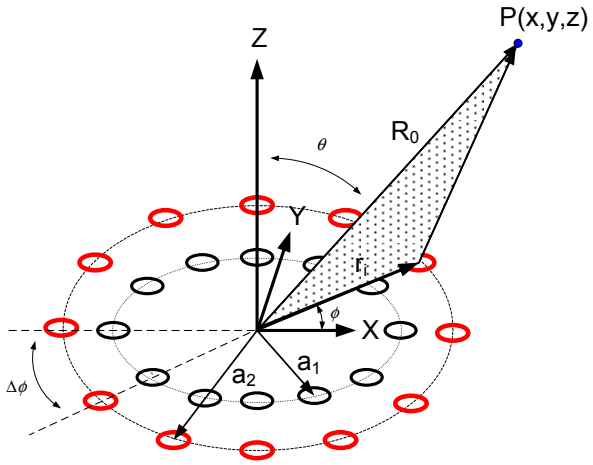

Fig.1. Theoretical two-ring concept of the dual beam array

A simplified mathematical model for the total field of the three-column two-ring array is

$$\hat{F}(\theta,\phi) = I_1 * \hat{E}_1(\theta,\phi) * \exp[\,jka_1 \sin\theta\cos(\phi-\Delta\phi)] + I_0 * \hat{E}_0(\theta,\phi) * \exp[\,jka_2 \sin\theta\cos(\phi)] + I_{-1} * \hat{E}_{-1}(\theta,\phi) * \exp[\,jka_1 \sin\theta\cos(\phi+\Delta\phi)] \quad (1)$$

Where,

$$\hat{E}_1(\theta,\phi) = \hat{E}_0(\theta,\phi-\Delta\phi) \quad (2)$$

$$\hat{E}_{-1}(\theta,\phi) = \hat{E}_0(\theta,\phi+\Delta\phi) \quad (3)$$

$\hat{E}_0(\theta,\phi)$ represents the element pattern of radiators on the center column. I_1 and I_{-1} are complex excitation coefficients for radiators 1 and -1. Radiuses of the two rings are a_1 and a_2, respectively. k is the wave number. $\Delta\phi$ is the angular spacing between radiating elements.

Fig. 2 shows the front and cross-sectional views of the 30-element, three-column, cylindrical sector array. The array is designed to operate in a typical wireless communication band,

1700 MHz to 2200 MHz. The radiating elements are aperture-coupled patches. Each of the three linear arrays is mounted on a separate reflector. Radius of the inside ring, a_1, is determined by the subtend angle of the two edge reflectors, α. Radius of the outside ring, a_2, is set and adjusted by the vertical displacement, D, which can be varied between -5mm to +25mm in the direction of the mechanical boresight direction.

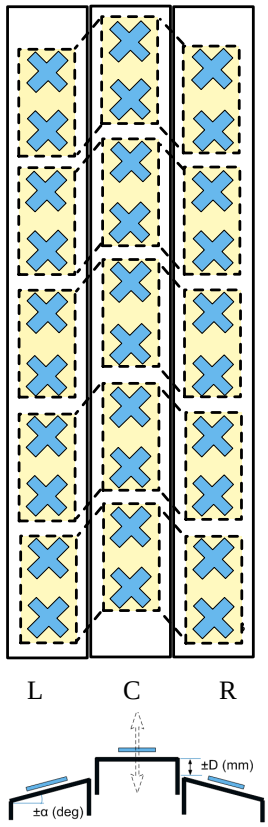

Fig. 2. Three-column array with adjustable center column

The relative slope of the two edge columns, α, with respect to the center column, is critical in achieving the required pattern shapes and beam cross-over loss. Typically, this angle is set between 20 deg to 30 deg with respect to the center column. With these parameters, the dual beam patterns can be maintained over a relatively broad frequency bandwidth. Fig. 3 shows a simulated 65˚ full coverage beam pattern and three independent narrow beams at 2200 MHz. For these analyses, the angle (α) is set at 20deg. The half-power-beamwidth (HPBW) of each individual narrow beam is approximately 33 deg, which provides combined azimuth coverage of 65 degree for a typical cell sector.

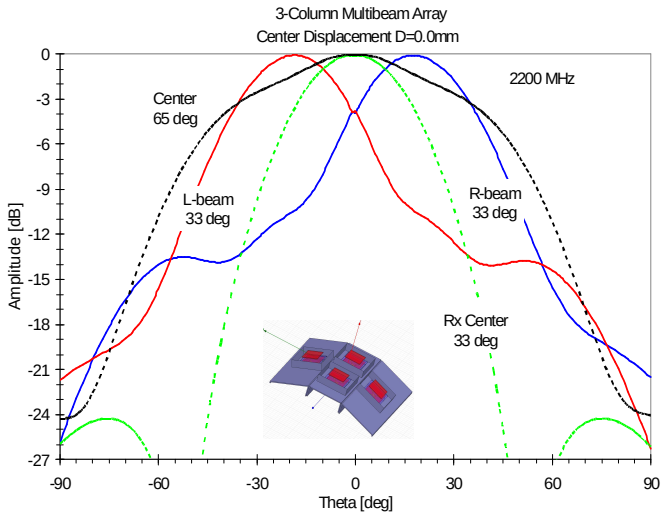

Fig. 3. Simulated beam patterns of the three-column array

With the displacement distance of the center column set at D=0mm (reflector surface of the center column levels with the top edges of the two edge columns), the three narrow beams and the 65˚ broad beam pattern can be formed using the following amplitude and phase excitations:

Beam	Left Array (L)	Center Array (C)	Right Array (R)
Left 33˚	(1, 0˚+Δφ)	(0.74, 0˚)	(0.34,-180˚+Δφ)
Center 33˚	(0.5, 0˚+Δφ)	(1.0, -30˚)	(0.5, 0˚+Δφ)
Right 33˚	(0.34,-180˚+Δφ)	(0.74, 0˚)	(1.0, 0˚+Δφ)
65˚ Beam	(0.5, -45˚)	(1.0, 0˚)	(0.5, -45˚)

Table I. Amplitude and Phase excitations for various beams

Where Δφ represents an additional phase adjustment, which can be introduced into the excitation by addition of a fixed line length on the feed line, or varying the relative displacement distance of the center column, D. This adjustable phase allows further optimization of beam parameters such as the beam cross-over losses and pattern discrimination.

III. BEAM FORMING CIRCUIT

Figure 4 shows amplitude and phase excitations of the 3-to-2 beam forming network for the dual beam patterns. Figure 5 and 6 show the equivalent signal diagram and the implementation of the compact dual beam former using micorstrip transmission line method.

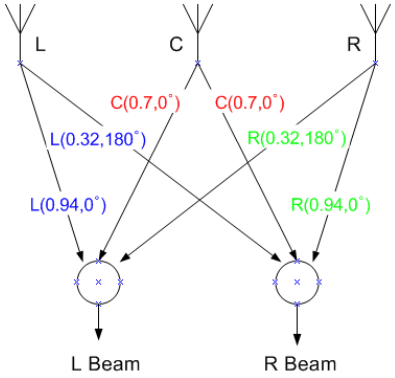

Fig. 4. Excitations function of the dual beam former

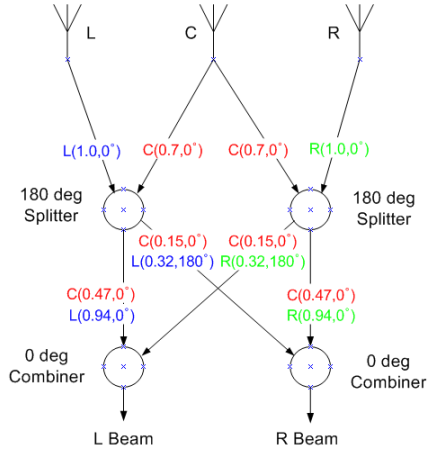

Fig.5. Equivalent excitation signal diagram of the dual beam former

The proposed 3-to-2 beam former is implemented using two unequally-split 180deg splitters and two in-phase Wilkinson combiners. This simple implementation has an added advantage of excellent isolations between antenna ports as shown in Fig.7 (pattern pending), simulated results (Agilent ADS). These merits are inherent result of port cancellation at the sum and difference ports of the 180 deg splitters.

Another significant advantage of this implementation is the low beam-split signal losses. Each of the dual beams are formed using a 180-deg splitter (10 dB) on the corresponding edge column and a 3dB (0 deg) splitter on the center column. The total signal loss due to the beam split is less than 0.5 dB in comparison to the single beam case (center 33˚), which has an excitation taper of (0.5, 1.0, 0.5). This is a direct result of the optimum phase and amplitude tapers from the array configuration. Furthermore, the path loss is also minimized because of the compact circuit design.

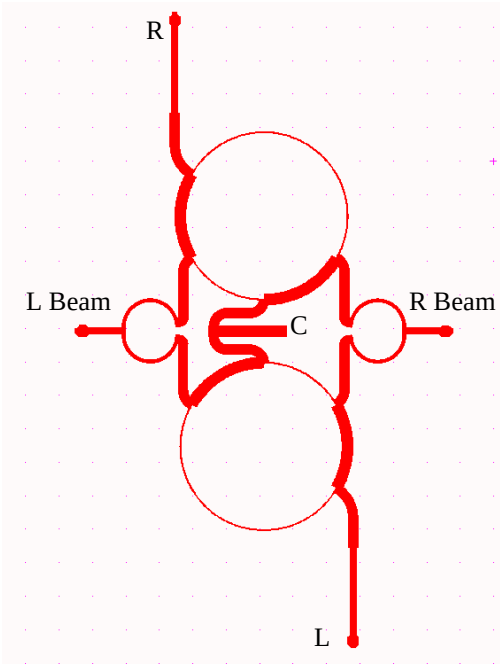

Fig. 6. Microstrip implementation of the compact dual beam former

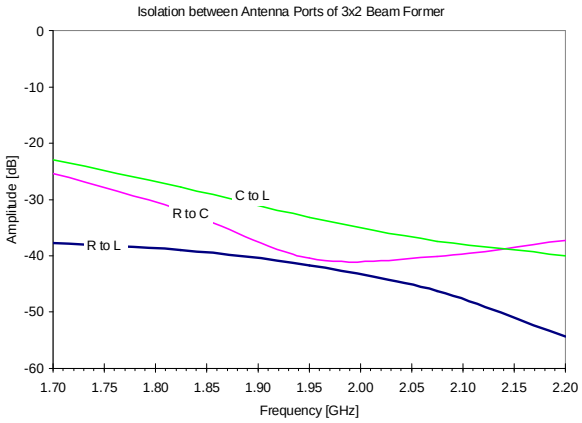

Fig. 7. Isolation between antenna ports of dual beam former

IV. Simulation Results

A 4-element sub-array model of the three-column array is simulated using the Ansoft 3D full-wave Finite Element Method (FEM) HFSS. For these analyses, the subtend angle is set to 20deg. Fig. 8 and 9 show the simulated azimuth patterns at 1700 MHz and 2200 MHz with the displacement distance (D) set at 0mm.

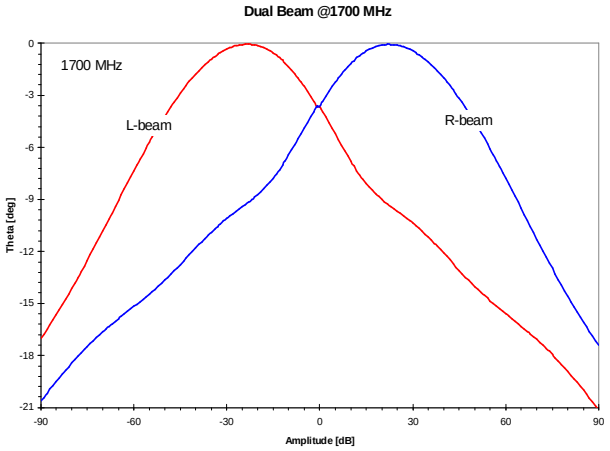

Fig. 8. Simulated dual beam patterns at 1700 MHz

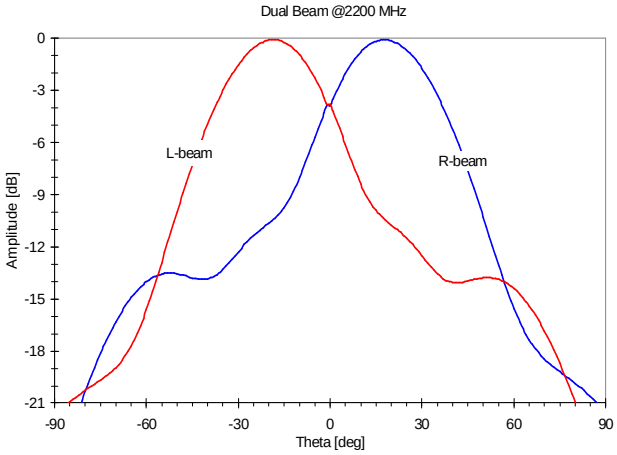

Fig. 9. Simulated dual beam patterns at 2200 MHz

The beam cross-over loss at azimuth=0 deg is between 3.5dB@1700 MHz to 3.7dB@2200 MHz When the displacement distance D is set at 0mm. These beam patterns and the cross-over losses can be varied by introducing an additional phase offset between the center column and the two edge columns using the adjustable displacement feature of the array. For comparison, Fig 10 shows the dual beam patterns for the displacement distance at -5mm, 0mm, and +15mm.

For displacement distance (D) between -5mm and +15mm, the beam cross-over loss is varying between -1.6dB to -4.9 dB. The lowest beam cross-over loss is -1.6 dB when the displacement distance is at D=-10mm. This low cross-over loss, however, comes at the expense of pattern discrimination performance (4dB at beam peak).

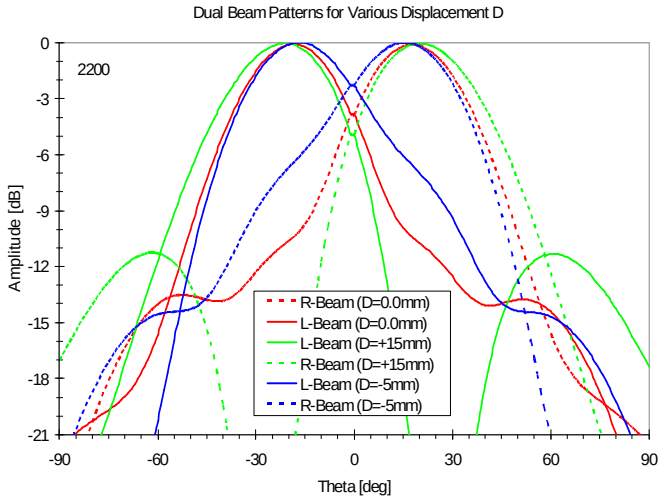

Fig. 10. Dual beam patterns for various displacement distance D

On the other hand, at D=+15mm, the dual beams has an optimum pattern discrimination of over 24dB at the expense of the beam cross-over loss of -4.9dB. The following table summarizes the dual beam performances for various displacement distance D.

Displacement Distance	Cross-over Loss	Discrimination At Peak	HPBW (deg)
D=-10 mm	-1.6 dB	4 dB	36
D=-5.0mm	-2.3 dB	6.5 dB	35
D= 0.0mm	-3.7 dB	10.5 dB	33
D=+15mm	-4.9 dB	24 dB	35

Table II. Pattern parameters for various displacement distance D

This feature allows one to optimize, for instance, performance at hand-over point (cross-over) or interference discrimination, as required.

VII. Measured Results and Comparisons

Fig. 11 show the prototype of the dual-beam array constructed based on the principle of the three-column variable beamwidth array. Five 3x2 microstrip BFNs are used to feed the 30-element array. BFN Outputs of the left (L) and right (R) beams are combined in two separate 1-to-5 RET (remote elevation tilt) phase shifters for separate elevation control. This allows beam tilt in elevation plane between 0 and 7 deg.

Antenna patterns of the array were measured in the Powerwave spherical near-field chamber in Santa Ana, California.

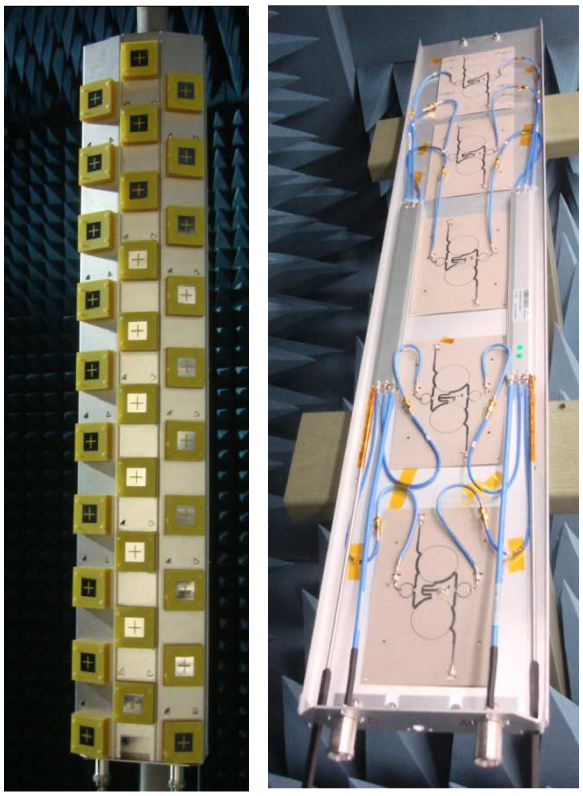

Fig.11. 3-Column Dual Beam Array and BFN Feeds

Fig. 12 shows a typical azimuth beam patterns (2150 MHz) of the array when the RET is set to 0 deg and center displacement D=0mm. In this case, the measured HPBW are approximately 31deg with cross over loss of about -4.9 dB. The array has very low cross-polar field components, well below -20 dB.

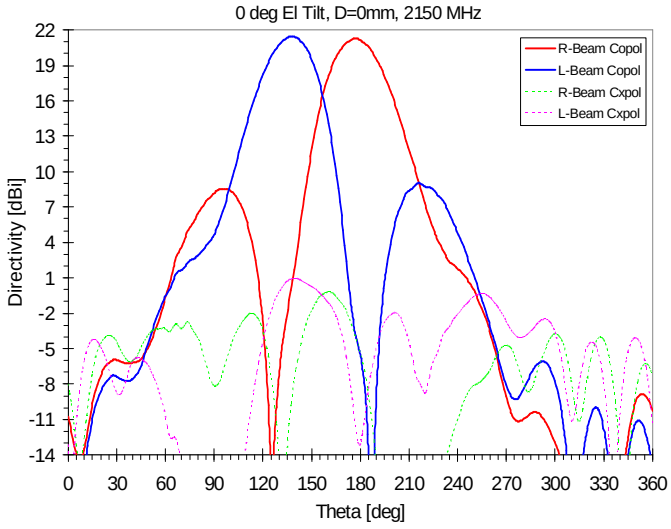

Fig.12. Measured azimuth beam patterns at 2150 MHz

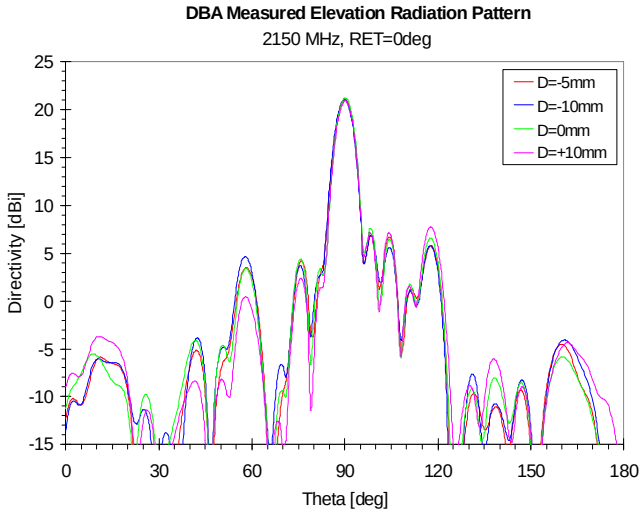

Fig.13. Measured elevation beam patterns at 2150 MHz

Fig. 13 gives typical elevation patterns of the array at 2150 MHz when RET=0deg. The offset distance does not seem to affect the main beam pattern in the elevation plane significantly. However, SLL tend to increase as the offset distance decreases.

Fig. 14 to 17 compare HFSS simulations and measured patterns (1700 MHz and 2200 MHz) in the azimuth plane for D=0.0mm and -5.0mm. These results show generally good correlations between the simulations and measured results. However, the HPBW is somewhat better correlated when the displacement D is above 0 mm and the cross-over loss is better predicted when D is below 0mm.

VII. CONCLUSIONS

An adjustable, dual beam antenna array, along with a compact, low-loss beam former (pattern pending) is presented for the wireless base station applications. This structure produces two symmetrical narrow beams with respect to the azimuth boresight within a cellular sector. Radiation patterns of the two beams are adjustable for optimization of the coverage of a cellular sector to minimize beam-split loss, or to optimize pattern discrimination and HPBW performance. This method allows an effective increase in the overall network capacity as a result of low-loss and narrow beam patterns.

A full array prototype was built and radiation patterns were measured in the Powerwave spherical near-field range (Santa Ana). Results are correlated with EM (HFSS) simulations.

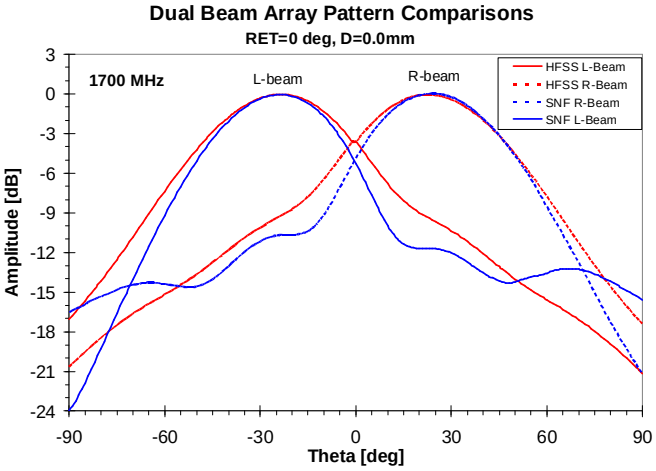

Fig.14. Pattern comparison at 1700MHz, D=0.0mm

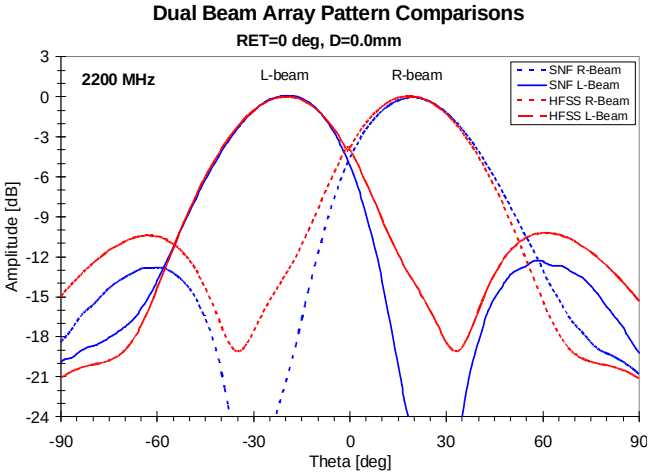

Fig.15. Pattern comparison at 2200 MHz, D=0.0mm

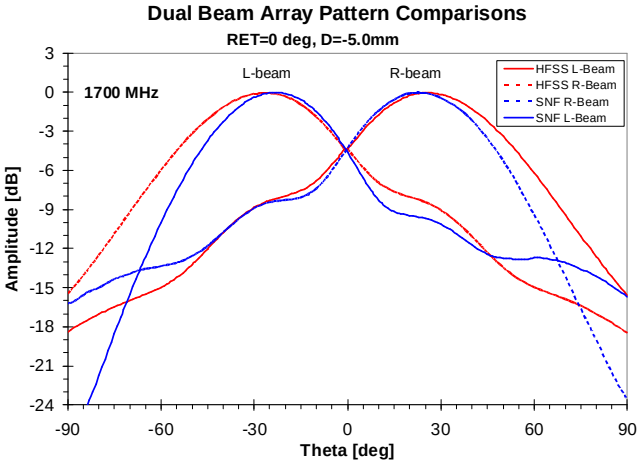

Fig.16. Pattern comparison at 1700 MHz, D=-5.0mm

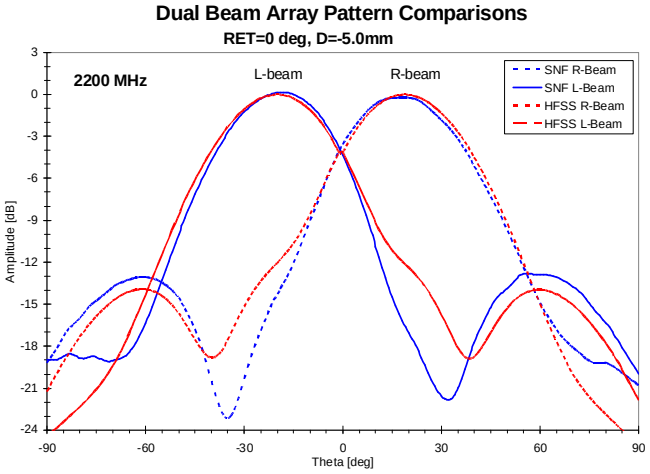

Fig.17. Pattern comparison at 2200 MHz, D=-5.0mm

REFERENCES

[1] R.J. Mailoux, *Phased Array Antenna Handbook*, second edition. Boston, MA: Artech House, 2005.

[2] R.C. Hansen, *Phased Array Antennas*. New York: John Wiley & Sons, 2005.